Science of the Total Environment 796 (2021) 149011

Contents lists available at ScienceDirect

Science of the Total Environment

journal homepage: www.elsevier.com/locate/scitotenv

Research Paper

A multi-proxy record of hurricanes, tsunami, and post-disturbance ecosystem changes from coastal southern Baja California

Qiang Yao [a,*], Kam-biu Liu [a], Yijing Wu [b], Alejandro Antonio Aragón-Moreno [a,c,**], Erika Rodrigues [d], Marcelo Cohen [d], Adriana V. de Souza [d], Luis M. Farfán [e], Jose Luis Antinao [f]

[a] Department of Oceanography and Coastal Sciences, College of the Coast and Environment, Louisiana State University, Baton Rouge, LA 70803, USA
[b] School of Ocean and Earth Science, Tongji University, 1239 Siping Road, Shanghai 200092, China
[c] Tecnológico Nacional de México, I. T. Chetumal, Av. Insurgentes 330, Chetumal, 77013, Quintana Roo, Mexico
[d] Laboratory of Coastal Dynamics, Graduate Program of Geology and Geochemistry, Brazil Federal University of Pará, Belém, PA, Brazil
[e] Centro de Investigación Científica y de Educación Superior de Ensenada, Unidad La Paz, Baja California Sur, Mexico
[f] Indiana Geological and Water Survey, Indiana University, 420 N Walnut St., Bloomington, IN 47404, USA

HIGHLIGHTS

- This study reveals a historical tsunami and hurricane record over Baja California.
- Sediment cores were used to study environmental responses to disturbance events.
- Multi-proxy results revealed four paleo-hurricanes and one paleo-tsunami.
- Tsunami run-up and backwash deposits each have specific characteristics.
- The current ecosystem and terrain is likely resulted from the ~530 cal yr BP tsunami.

GRAPHICAL ABSTRACT

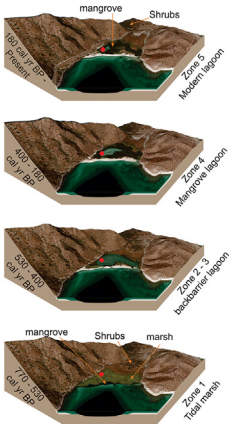

ARTICLE INFO

Article history:
Received 9 April 2021
Received in revised form 8 July 2021
Accepted 9 July 2021
Available online 14 July 2021

Editor: Fernando A.L. Pacheco

Keywords:
Extreme events
Palynology
Multi-proxy record
Mangroves
Baja California

ABSTRACT

Tsunamis and hurricanes are two earth surface processes that can dramatically impact coastal landforms and ecosystems. This study uses a combination of palynological, grain-size, X-ray fluorescence, and loss-on-ignition analyses, short-lived isotopic and radiocarbon dating, and statistical analysis to differentiate the tsunami and hurricane deposits, establish a Late-Holocene record of extreme events, and document the landscape and vegetation transformation in response to disturbance events and environmental changes from a small coastal lagoon in Baja California, Mexico. Prior to ~530 cal yr BP, Playa Los Cocos was occupied by a short-hydroperiod tidal marsh bounded by desert vegetation on the surrounding hillslopes. At ~530 cal yr BP, a tsunami created a backbarrier lagoon and introduced mangrove propagules from other coastal localities, and the lagoonal environment and substrates also provided suitable habitats for red mangroves to proliferate. Once established, red mangrove populations rapidly expanded until ~180 cal yr BP, when modern human activities diminished the mangrove forest in our study area. Overall, the multi-proxy dataset revealed four hurricane events at ~770, ~600, ~280, and ~0 cal yr BP, and one tsunami event at ~530 cal yr BP. The hurricane deposits were preserved in the form of fluvial and slope-wash deposits characterized by low organic and water contents, low concentration of marine elements, and high concentration of terrestrial elements. The tsunami run-up deposits are

* Corresponding author.
** Correspondence to: A. A. Aragón-Moreno, Tecnológico Nacional de México – I. T. Chetumal, Av. Insurgentes 330, Chetumal, 77013, Quintana Roo, Mexico.
E-mail addresses: qyao4@lsu.edu (Q. Yao), aaragon@ecosur.edu.mx (A.A. Aragón-Moreno).

https://doi.org/10.1016/j.scitotenv.2021.149011

characterized by abundant broken and intact sea shells, high content of carbonate and marine elements, low concentration of terrestrial elements, and sharp basal contact with the underlying sediments. The tsunami backwash deposits are characterized by a mixed physical and chemical signature resembling both marine and terrestrial sediments. Results also suggest that both hurricanes and tsunamis can help propagule dispersal and create suitable coastal habitats favorable for the spread and proliferation of mangroves in a desert coastal environment.

1. Introduction

Tsunamis and tropical cyclones are two main earth surface processes that can significantly alter coastal landforms and ecosystems. Recent events such as Hurricane Katrina (2005, North Atlantic), Typhoon Haiyan (2013, Western Pacific), and the Indian Ocean (2004) and Tohoku (2011) Tsunamis had dramatic biophysical and societal impacts on coastal environments in different parts of the world. Therefore, identifying these disturbance events in the geological record and documenting their long-term ecological impacts have broad significance in understanding and predicting the coastal landscape evolution worldwide. During the past few decades, many researchers have studied tsunami deposits in sedimentary records across the Western Pacific (Minoura and Nakaya, 1991; Minoura et al., 2001; Nanayama and Shigeno, 2006), the North American - Pacific Plate boundary (McCloskey et al., 2015; Ramirez-Herrera et al., 2007; 2020), and other tectonically active places worldwide (Peters and Jaffe, 2010; Chagué-Goff et al., 2011; Goff et al., 2012, 2020). Generally speaking, typical characteristics of tsunami deposits found in onshore environments include signs of sea-water intrusion, wide-ranging size of allochthonous deposits, sharp basal contact, and poor sorting (Dawson and Shi, 2000; Dawson and Stewart, 2007).

Similarly, extensive studies have documented the physical and chemical signatures of hurricane deposits (e.g., Donnelly et al., 2001; Woodruff et al., 2008; Liu, 2004; Brandon et al., 2013; Wallace et al., 2014; Bregy et al., 2018; Yao et al., 2018, 2019). Nonetheless, many tectonically active coastal regions across the tropics and subtropics are impacted by both tsunamis and hurricanes. Because tsunami and hurricane deposits are produced by comparable physical processes and have similar sedimentary characteristics, few studies have successfully distinguished them in the sedimentary profile (Tuttle et al., 2004; Morton et al., 2007; Kortekaas and Dawson, 2007; Ramírez-Herrera et al., 2012; Horton et al., 2013). Hence, paleo-tsunami is still not well documented in geological record (Peters and Jaffe, 2010; Chagué et al., 2020; Engel et al., 2020), and studies documenting the depositional processes of tsunami-triggered backwash are rare (Dawson, 1994; Dawson and Stewart, 2007; Chagué-Goff et al., 2017).

The Baja California Peninsula in Northwestern Mexico, is positioned over the Gulf of California Transform Faults between the East Pacific Rise and San Andreas Fault (Fig. 1), where the tectonic boundaries between the North American Plate and the Pacific Plate slide past each other. Consequently, the region is known for its tsunamis and earthquake activities (Gonzalez-Yajimovich et al., 2007; Castro et al., 2017). Moreover, tropical storms and hurricanes also play a major role in the coastal morphological evolution of the peninsula. Although rare, episodic storms cause erosion on the rocky shorelines and bring heavy rainfall that dramatically alter the desert vegetation and terrain over Baja California (McDonald et al., 2003; Antinao et al., 2016). Furthermore, these distinctive geomorphological settings of the region contribute to a diverse climate ranging from mild Mediterranean climate in the northern peninsula to arid desert climate in the south (Case et al., 2002; Pérez-Cruz, 2006). The unique landscape and ecosystems of Baja California support a large variety of indigenous and endangered flora and fauna (Glover et al., 2020). Thus, the rich geological and biological diversity of Baja California draws attention from geologists, biologists, and ecologists around the globe.

Unfortunately, climate change and anthropogenic activities have posed significant threats to the arid ecosystems in the region (Underwood et al., 2009; Arianoutsou et al., 2012). In recent years, the peninsula is warming faster than most areas in North America (Bedsworth et al., 2018). Under the current prediction, the Mediterranean biome in the region will likely shift northward by the end of the 21st century (Seager et al., 2019; Glover et al., 2020), leaving the entire peninsula a subtropical desert. Hence, in order to project the regional vegetation dynamics under the warming climate, it is imperative to understand how the coastal ecosystem responds to environmental change. However, very few long-term ecological record from the region exist in the literature (Pérez-Cruz, 2013; Ezcurra et al., 2016; Figueroa-Rangel et al., 2016; Páez-Osuna et al., 2016). In particular, the impacts of tsunamis and hurricanes on coastal ecosystems and morphodynamics and the process of post-disturbance vegetation changes in tectonically active arid coastal regions, such as Baja California, have not been well documented. Thus, large data gaps exist in the literature.

Coastal lacustrine environments, especially lagoons surrounded by hillslopes in the desert region are particularly sensitive to record climatic and hydrological extremes, such as landslides, storm surges, and tsunamis (Antinao and Farfán, 2013). In this study, we present three sediment cores (Cocos-7, 9, and 11) retrieved from a small coastal lagoon at a dried fluvial valley in Playa Los Cocos, southern Baja California (Baja California Sur) and 20 surface samples from surrounding areas (Fig. 1). The objectives of this study are to utilize a combination of palynological, grainsize, X-ray fluorescence (XRF), and loss-on ignition (LOI) datasets, short-lived isotopic and radiocarbon dating, and statistical analysis to (1) reveal the sedimentary and geochemical characteristics of different endmember source sediments, (2) differentiate between tsunami and hurricane deposits and establish a Late-Holocene tsunami and hurricane record, (3) elucidate the tsunami backwash process based on a multi-proxy dataset, (4) document the long-term dynamics of desert coastal vegetation in response to environmental changes and disturbance events.

2. Regional setting

2.1. Study site description

The Baja California Peninsula, an elongated peninsula with an area of ~144,000 km^2, is bordered on the north by the U.S. state of California, on the west by the Pacific Ocean, and is separated from mainland Mexico by the Gulf of California (Fig. 1). Below the gulf's sea floor, the relative movement of the North American Plate and the Pacific Plate changes from moving away to sliding past each other, forming many transform faults characterized by a zigzag pattern, known as the Gulf of California Transform Faults (Stock and Hodges, 1989; Sedlock, 2003) (Fig. 1c). Originated along transform faults, mountain belts run through the center of the peninsula, exhibiting the aftermath of past tectonic activities. The mountains produce a rain shadow and extremely arid environment along the Gulf side of the peninsula, including our study area. Consequently, vegetation is sparse along the Gulf coast and comprises mainly of desert shrubs and herbs, especially of the families Papilionoideae and Asteraceae (Case et al., 2002; Martínez-López et al., 2019). Forest taxa such as pine (*Pinus*) and oak (*Quercus*) are more common on the mountains and on the Pacific side (Case et al., 2002).

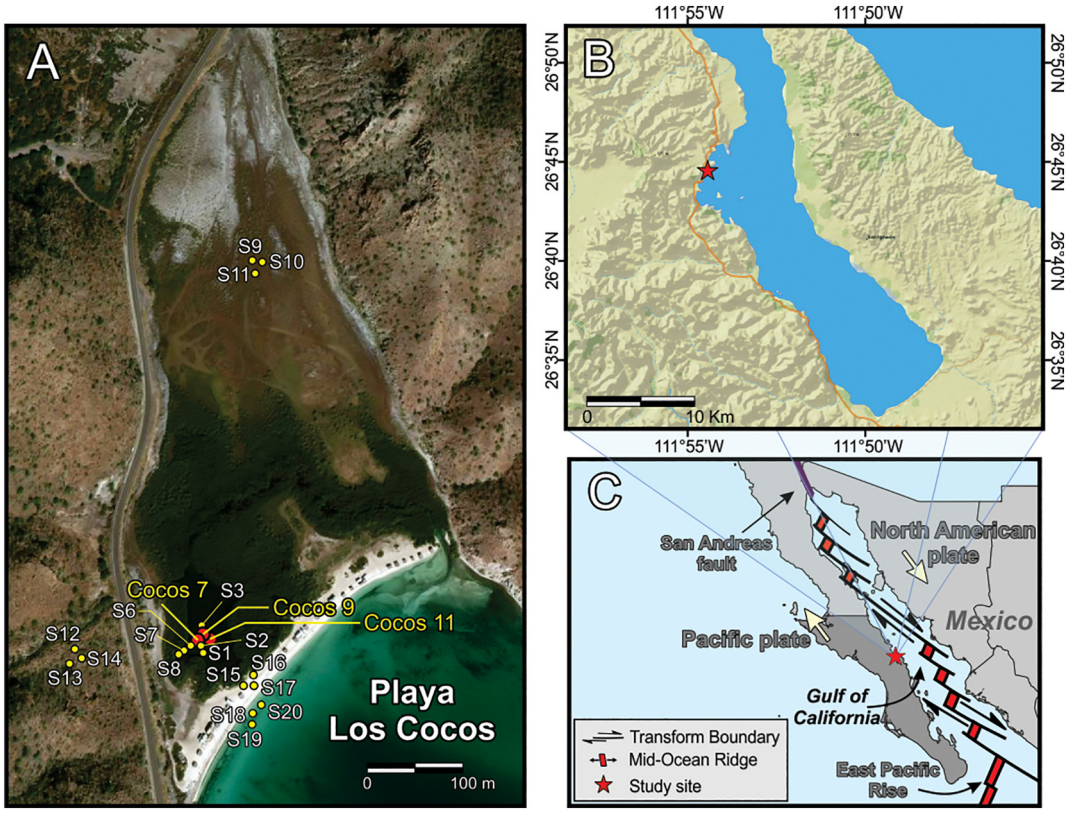

Fig. 1. Maps of the study area. (A) Laguna Los Cocos. Red dot marks the location of sediment cores. Yellow dots mark the locations of surface samples. (B) Bahia Concepcion. Red star marks Playa Los Cocos. (C) Gulf of California Transform Faults. (For interpretation of the references to color in this figure legend, the reader is referred to the web version of this article.)

Our study area, Playa Los Cocos (Fig. 1a) is a small bay (~550 m wide at the bay mouth) located in Bahia Concepcion (Concepcion Bay), southern Baja California (Fig. 1b). The coring site, Laguna Los Cocos, is a small lagoon (~5000 m^2) at the south end of Playa Los Cocos (Fig. 1a). The lagoon is situated in a dry fluvial valley bordered by hillslopes on the east and west sides and enclosed behind a barrier beach on the south side (Fig. 1a). A 300 m tidal inlet at the northeastern side of the bay connects the lagoon with Bahia Concepcion. Field measurements taken in March 2019 showed that salinity of the lagoon is 30‰. The depth of the lagoon is ~1 m at the center and gradually becomes shallower toward the edge. Previous studies indicated that rainfall induced by episodic tropical cyclones could be much more intense than that associated with monsoon or winter storms and serve as the primary source of regional moisture (McDonald et al., 2003; Antinao and McDonald, 2011; Antinao et al., 2016; Martínez-López et al., 2019). Precipitation record from an automated weather station operated by Mexico's Servicio Meteorológico Nacional (SMN) ~18 km to the north of our study site shows that the accumulated precipitation ranges from 1.5 to 369 mm, per year, with an average of only 110 mm during the past 97 years (1922–2016) (SMN, 2020). Currently, the lagoon is surrounded by red mangroves (*Rhizophora mangle*), with black (*Avicennia germinans*) and white mangroves (*Laguncularia racmosa*) growing on higher flats around its edges. Desert shrubs and herbs occupy the outer fringe of the bay and on the hills.

2.2. Instrumental and historical record of tropical cyclones and tsunamis in the region

The U.S National Oceanic and Atmospheric Administration (NOAA) Historical Hurricane Tracks database contains 67 years (1954–2020) of instrumental storm record for the Baja California peninsula (NOAA, 2020). The record shows that a total of 17 tropical cyclones made landfall near Playa Los Cocos (within 200 km radius) from 1950 to 2000 CE, an average return interval of ~3.8 years (Fig. 2b). These 17 tropical cyclones include nine tropical storms, seven category-1 hurricanes (Saffir-Simpson scale), and one category-3 hurricane – Olivia, which made landfall ~26 km to the north of our study site on October 14th, 1967 with sustained winds up to 200 km/h (NHC, 2015). It is the only one of two documented major hurricanes that ever made landfall on the Gulf side of Baja California.

Since the 21st century, a total of 15 tropical cyclones have made landfall near our study area (within 200 km radius) (Fig. 2a), an average return interval of ~1.3 years (NOAA, 2020). Among them, eight are tropical storms, three are category-1 hurricanes, three are category-2 hurricanes at landfall, and one major hurricane, Odile, which directly acrossed Cabo San Lucas on September 15th, 2014. It was tied with Hurricane Olivia for the most intense hurricanes ever hitting Baja California with sustained winds of 205 km/h at landfall (NOAA, 2020). Despite being the most intense recorded hurricane of the region, Odile was significantly weakened by the southwesterly wind shear and mountain belts of the peninsula when it moved northward. (Fig. 2a). Among other conditions, the orographic effect of the mountain belts likely weakened its influences when Odile passed Playa Los Cocos ~50 km to the west.

Instrumental (NGDC/WDS, 2017) and historical records (Farreras and Sanchez, 1991; Ramírez-Herrera et al., 2019) documented 13 local and regional tsunamis (< 200 km from the source) generated by tectonic and geological activities in the Gulf of California since the 19th century (Fig. 2c & d). Because these tsunamis were recorded exclusively from areas with human occupation and tidal gauges, more tsunamis likely impacted Baja California during the early period. Among the 13 tsunamis, the August 27th 1810 tsunami was caused by an earthquake near Loreto (Ramírez-Herrera et al., 2019), one of the largest cities in Baja California Sur located at ~100 km south of our study site. This 7.4 Mw earthquake devastated the settlement and triggered a large basin-

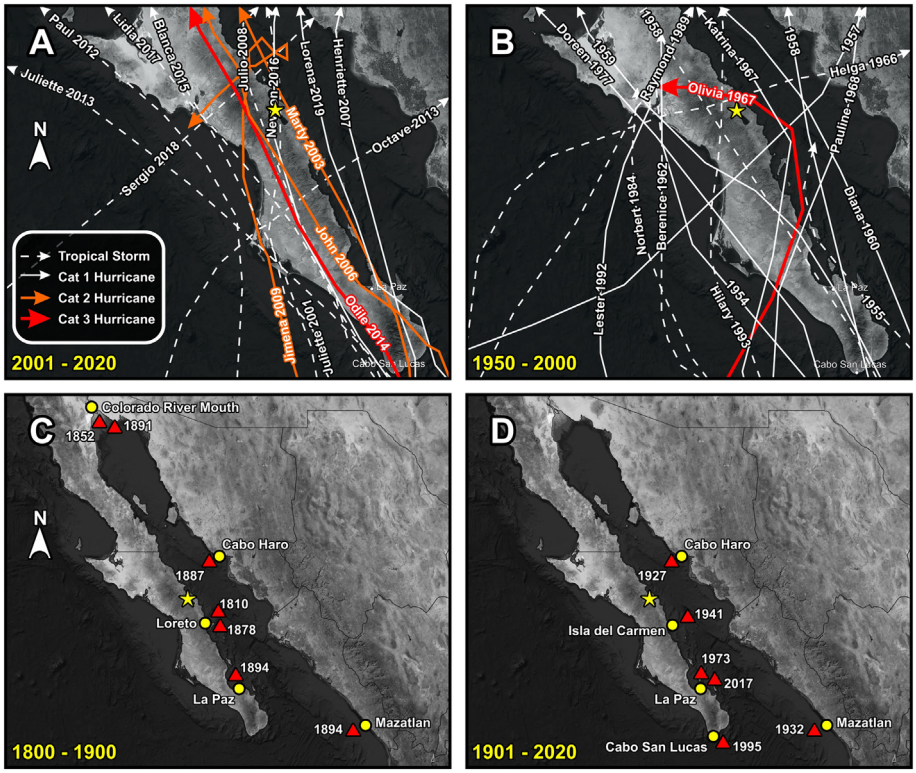

Fig. 2. Instrumental and historical record of storm tracks (A) and (B) (NOAA, 2020) and local tsunamis (C) and (D) (Farreras and Sanchez, 1991; Ramírez-Herrera et al., 2019; NGDC/WDS, 2017) of Baja California Peninsula and surrounding area. Yellow star marks Playa Los Cocos. Red triangle and yellow circle in (C) and (D) marks the approximate location of the tsunami and affected city (area). (For interpretation of the references to color in this figure legend, the reader is referred to the web version of this article.)

wise tsunami (up to 20 m) that affected over 200 km of the Loreto-La Paz coast (Suter, 2018; Ramírez-Herrera et al., 2019) (Fig. 2c). Beyond the instrumental period, sedimentary and geochemical record revealed three large turbidites likely attributed to earthquakes occurring at 4900, 2800, and 1500 cal yr BP (Gonzalez-Yajimovich et al., 2007), and one large tsunami occurring at 1100 cal yr BP (McCloskey et al., 2015) near the city of La Paz. No evidence of large basin-wide tsunami has been revealed from sedimentary record for the last 1000 years (Gonzalez-Yajimovich et al., 2007; McCloskey et al., 2015). More details regarding the above-mentioned tsunami events are described in Supplementary Content (Table S1).

3. Materials and methods

3.1. Field work

In March 2019, three sediment cores, Cocos-7 (79 cm), Cocos-9 (48 cm), and Cocos-11 (50 cm) were recovered from Laguna Los Cocos (Fig. 1a). The main core, Cocos-7, was retrieved by pushing an aluminum push corer (8 cm diameter) until it reached an impenetrable substrate near the center of the lagoon (26°44′35.79″N, 111°54′4.79″W). Cocos-9 &11 were retrieved using a Russian peat borer (5.5 cm diameter) to duplicate and verify Cocos-7. Hence, Cocos-9 was taken right next to Cocos-7. Cocos-11 was recovered at a nearby site slightly further to the east (26°44′35.68″N, 111°54′4.77″W). In addition, 20 surface samples (S1-S20) were retrieved in and around the lagoon (Fig. 1a). Among them, two samples (S4 and S5) were taken from the same location as core Cocos-7 & 9. The other 18 samples were taken from the lagoon (S1-S3 and S6-S8), fluvial plain (S9-S11), hillslopes (S12-S14), beach (S15-S17), and nearshore environment (S18-S20). All cores and surface samples are currently stored in a cold room (4 °C) at Louisiana State University. GPS coordinates of all cores and surface samples can be found in Supplementary Content (Table S2).

3.2. Multi-proxy analyses

X-ray fluorescence (XRF) and loss-on-ignition (LOI) analyses were performed for all surface samples and cores at 1 cm interval. An Olympus Innov-X DELTA Premium XRF analyzer was used for XRF analysis, following standard procedures (Yao et al., 2020a & 2020). The elemental concentrations (ppm) of eight common elements were reported in this study. LOI analysis followed the procedures described in Dean (1974). It reveals the % water (wet weight), % organics (dry weight), and % carbonates (dry weight) of the sediment profile. Grain-size analysis was performed for all surface samples and at a 2 cm interval for Cocos-7 and 5 cm interval for Cocos-9 and Cocos-11, using a Beckman Coulter particle size analyzer (0.04–2000 μm range). The sample pretreatment followed the procedures described in Wang et al. (2019). The overall clay (< 2 μm), silt (2–63 μm), and sand (63–2000 μm) fractions were reported for each sample.

Palynological analysis was performed on all three cores at 2 to 5 cm intervals. All pollen samples were processed using standard laboratory procedures described in Aragón-Moreno et al. (2018, 2012). Published pollen keys by Yao and Liu (2018) and Vargas-Sánchez et al. (2016) were used to aid the pollen identification. Over 300 grains of pollen and spores were counted for each sample. The concentrations of algae, foraminifera linings, dinoflagellates tests, and charcoal fragments (>10 μm in size) were also reported for every sample. One tablet containing ~20,583 *Lycopodium* spores (L_c) was added to every sample as an exotic marker to aid the calculation of pollen concentrations (grains/cm^3).

3.3. Chronology

Thirteen samples were sent to ICA Inc., in Florida, for AMS ^{14}C dating (Table 1). Among them, six samples consist of leaves and plant fragments. For sample intervals where plant macrofossils are absent,

approximately 5 g of sediments were sieved and inspected under a dissecting microscope to remove shells and roots from bulk clastic and fine organic fraction of the sediments. These sieved bulk sediments were used for AMS ^{14}C dating. The top 50 cm of core Cocos-7 was sent to State Key Laboratory of Marine Geology, Tongji University, China for ^{210}Pb and ^{137}Cs dating at 1 cm interval. Gamma-ray measurements were performed on a HPGe well type γ-ray detector (GWL-120-15-LB-AWT, AMETEK). Excess ^{210}Pb ($^{210}Pb_{ex}$) activity was determined by subtracting the supported ^{210}Pb ($^{210}Pb_{su}$, equivalent to 226Ra) from total ^{210}Pb ($^{210}Pb_t$). The uppermost sediments (0–5 cm) were measured in the detector for 96 h and the other sample intervals were measured for 48 h. Details regarding the pretreatment and analyses for radiocarbon and short-lived isotope samples are described in Supplementary Content. Chronology of the main core Cocos-7 was established using *BACON* version 2.2 (default priors and settings) (Blaauw, 2010). All radiocarbon dates were converted to calibrated year before present (cal yr BP) using Calib 7.2 (Stuiver et al., 2020) and rounded to the nearest decade.

3.4. Statistical analyses

Principal component analysis (PCA) was performed on the XRF and LOI datasets of the surface samples using C-2 version 1.7.7 (rotate axes, center data by variables, standardize data by variables) to reveal the distribution of endmember source sediments in relation to their sedimentary and geochemical parameters. The PCA provides a foundation to categorize various proxies into statistically meaningful groups, which can then be used to reveal the characteristics of different sediment endmembers.

3.5. Graphic simulation

The Global Mapper v.18 was used to produce the model simulation of vegetation and geomorphological development at Playa Los Cocos. The modern terrain is based on QuickBird satellite images (Jan/2021), downloaded from Google Earth (2.44 m resolution), and digital elevation model derived from Shuttle Radar Topography Mission (SRTM) data, downloaded from the United States Geological Survey (USGS) (Gorelick et al., 2017). The three-dimensional paleoenvironment simulations were created from satellite image and edited in Corel Photo-Paint X6 following the interpretation of multi-proxy data. Finally, these simulated satellite images were merged with the modern digital elevation model of the study area.

4. Results

4.1. Numerical analysis of endmember source sediments

Grain-size, LOI, and XRF datasets of surface samples exhibit distinct differences among endmember source sediments (Fig. 3a). The lake sample group (S1-S8) shows the highest values of %Water, %Organic, and Br, and lowest values in %Carbonate, Ca, and Sr among all surface sample groups. Both the fluvial plain (S9-S11) and the hillslope (S12-S14) groups are characterized by high concentrations of Zr, K, Fe, and Ti, and low values in all other parameters. Samples in the beach and offshore groups consist mostly of sand. The beach group (S15-S17) has the highest values of %Carbonate, Ca, and Sr among all sample groups. The nearshore group (S18-S20) has the lowest concentrations of Zr, K, Fe, and Ti, and high values of %Carbonate, Cl, Sr, and Br.

On the PCA biplot showing the distribution of endmember source sediments in relation to LOI and XRF results (Fig. 3b), the first two principal components (PC) account for 51.05% and 35.8% of the variance, respectively (Tables S3–S4). Along the PC1 axis, all terrestrial indicators (Fe, Ti, K, and Zr) (Haug et al., 2001; Van Soelen et al., 2012; Yao et al., 2020a) have the highest positive loadings and close association with the fluvial and hillslope groups, whereas all marine indicators (%Carbonate, Sr, Ca, Cl, and Br) (Ramírez-Herrera et al., 2012; Liu et al., 2014; Ercolani et al., 2015; McCloskey et al., 2018) have the lowest negative loadings and close association with the beach and nearshore sample group. Hence, PC1 clearly represents a salinity gradient whereby salinity decreases from the negative end toward the positive end. On PC2, the beach samples are closely

Table 1
Radiocarbon dating results for core Cocos-7, Cocos-9, and Cocos-11. Samples deemed unacceptable by the Bayesian model are marked in grey color.

Sample ID	Sample type	Conventional age (BP)	Calibrated age (cal yr BP)	2-Sigma calibration (cal yr BP)
Cocos-7 (17 cm)	**Leaf**	**modern**	**modern**	**N/A**
Cocos-7 (25 cm)	Bulk sediments	990 +/− 40	870	960–900 (41.9%) 890–790 (58.1%)
Cocos-7 (40 cm)	**Plant tissue**	**370 +/− 30**	**430**	**500–420 (54.7%) 400–320 (45.3%)**
Cocos-7 (55 cm)	**Leaf**	**500 +/− 30**	**530**	**550–500 (100%)**
Cocos-7 (60 cm)	Seed	1150 +/− 40	1050	1130–960 (89.7%), 1150–1140 (2.1%), 1180–1160 (8.2%)
Cocos-7 (72 cm)	**Plant tissue**	**740 +/− 30**	**680**	**720–650**
Cocos-7 (79 cm)	**Leaf**	**760 +/− 50**	**700**	**770–760 (3%), 750–650 (93.6%), 580–570 (3.4%)**
Cocos-9 (35 cm)	Seed	1020 +/− 40	940	1060–1020 (4.2%), 1010–890 (76.5%), 870–790 (14.8%)
Cocos-11 (20 cm)	Bulk Sediment	1680 +/− 40 BP	1570	1700–1660 (16.6%), 1640–1510 (76.3%), 1420–1450 (5%)
Cocos-11 (45 cm)	**Leaf**	**860 +/− 30**	**770**	**1050–1080 (6.1%), 1160–1230 (86.3%), 1240–1260 (7.6%)**
Cocos-11 (46 cm)	**Bulk Sediment**	**Not reported**	**N/A**	**N/A**
Cocos-11 (47 cm)	**Bulk Sediment**	**Not reported**	**N/A**	**N/A**
Cocos-11 (48 cm)	**Bulk Sediment**	**Not reported**	**N/A**	**N/A**

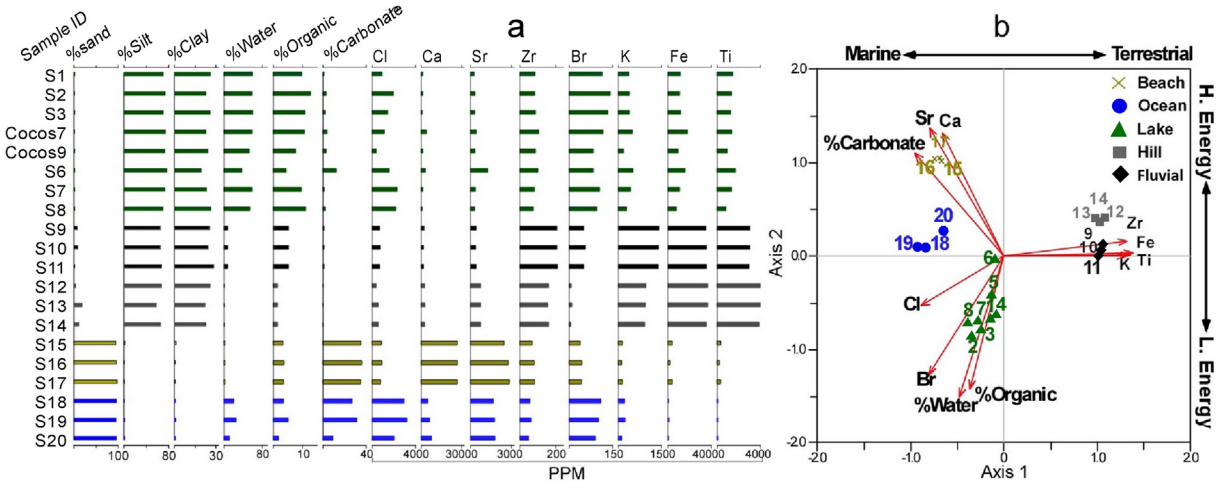

Fig. 3. a). Grain-size, LOI, and XRF dataset of surface samples. b). PCA biplot showing the distribution of surface sample groups in relation to various proxies. Each sample group is marked by a different color.

associated with marine indicators (%Carbonate, Sr, and Ca), while Br, % Water, and %Organic have the lowest negative loadings and close association with the lake sample group (Fig. 3b). Since deposits from stable, low-energy environments typically have higher water and organic contents than those from dynamic environments, PC2 likely indicates an energy gradient from bottom to top.

4.2. Radiocarbon and short-lived isotopic dating results

Short-lived isotope results show that ^{137}Cs activity from all sample intervals in Cocos-7 had lower than the 48 h minimum detectable concentrations (MDC_{48h}), and ^{137}Cs in the core top (0–5 cm) were lower than the MDC_{96h}. Similarly, both $^{210}Pb_t$ and $^{210}Pb_{su}$ activity from all layers in Cocos-7 were lower than the MDC_{48h}. By extending the counting time, the $^{210}Pb_{su}$ (via ^{226}Ra at 351.9 keV) show detectable activities of 0.63 ± 0.04 and 0.67 ± 0.04 dpm/g at 0–1 cm and 4–5 cm, respectively. While only the top 1 cm has detectable $^{210}Pb_t$, therefore $^{210}Pb_{ex}$ activity of 0.99 ± 0.04 dpm/g was derived at 0–1 cm. Collectively, radionuclides analysis suggests that the surface (0–1 cm) of Cocos-7 was dated back to the mid-1950s, and the rest of the sediment interval were older than 100 calendar years. Since this study use 1950 CE as 0 cal yr BP, the surface of Cocos-7 (0–1 cm) is assigned as 0 cal yr BP in the chronology model. Short-lived isotope results are illustrated in Supplementary Content (Fig. S1).

Among the thirteen ^{14}C samples, three samples taken from 46, 47, and 48 cm at the bottom of core Cocos-11 did not yield graphite due to low organic content. Results of the other ten samples are reported in Table 1 and Fig. 4. The Bayesian model deemed two samples (25 cm and 60 cm) from Cocos-7 as invalid. Two other dates from Cocos-9 (35 cm) and Cocos-11 (20 cm) were also deemed invalid based on stratigraphic correlation discussed in later sections. The Bayesian age model of Cocos-7 is illustrated in Supplementary Content (Fig. S2).

4.3. Stratigraphy, sedimentary and geochemical dataset

The multi-proxy analyses and visual inspection revealed that core Cocos-7 consists of five different types of sediments (Fig. 4). Upon visual inspection in the field, the top 40 cm is reddish brown color, and the rest of the core is grey to dark grey color. The bulk of the core consists of silty sand. Finer silt layers occur at 0–2 cm (H-4), 22–25 cm (H-3), 45–53 cm (T-b), and 63–66 cm (H-2). Sediments in these silt layers generally have higher contents of terrestrial elements (Zr, K, Ti, Fe) and higher values of Fe/Sr, a normalized parameter showing terrestrial vs. marine fraction in sediments. In particular, the silt layer at 45–53 cm has very low water content. Sand and fine sand with high contents of carbonate, Ca, and Sr and low contents of terrestrial elements occur at 53–61 cm (T-a). This sand layer has sharp basal contact with the silty sand layer beneath it and contains plenty of broken shells and a few shells of *Mulinia* sp. Intact shells of *Nassarius* snails are present in the three silt layers (H-1, T-b, and H-2) and throughout the bottom 10 cm of the core. An intact shell of Mexican Deep Scallop (*Euvola vogdesi*) is present between the silt and silty sand layers at 45 cm. It is worth noting that the concentration of Cl is significantly higher in the top 15 cm of the core. In addition, the lagoon bottom contains ~10 cm of unconsolidated mud at the surface (see Fig. S3 in Supplementary Content). Unfortunately, this mud layer was in liquid state and not preserved in core Cocos-7 upon core opening in the laboratory.

Core Cocos-9 consists of three types of sediments (Fig. 4). The top 10 cm is the same reddish brown color as the top 40 cm in core Cocos-7. Fine sand with sharp basal contact, abundant broken shells, and some *Nassarius* snails occur at 20–40 cm (T-a). Silty sand layers occur at 0–10 cm, 40–43 cm, and imbedded in the fine sand layer. Silt layers occur at 10–20 cm (T-b) and the bottom of the core (43–48 cm) (H-2). *Nassarius* snails are present in both silt layers.

Core Cocos-11 (Fig. 4) consists of five types of sediments. The top 22 cm (T-a) consists of fine sand with a coarse sand layer at 5–7 cm. This sand layer has sharp basal contact with the silty sand layer below and contains plenty of broken shells and a few *Nassarius* snails and *Mulinia* shells. Silty sand layers occur at 22–38 cm and 41–45 cm. Silt layers are found at 38–41 cm (H-2) and 45–50 cm (H-1). *Nassarius* snails are present throughout the bottom 10 cm of the core. The XRF and LOI characteristics of the various sediment types in core Cocos-9 and Cocos-11 closely resemble those of Cocos-7. In general, coarser sediments (sand and fine sand) have higher content of marine elements and carbonate, whereas finer grain sediments (sandy silt and silt) are rich in terrestrial elements but have lower content of water (Fig. 4). A detailed illustration of core stratigraphy is presented in Supplementary Content (Fig. S4).

4.4. Pollen data

A total of 67 pollen, spore, and plankton taxa were identified from the cores, and palynomorphs occurred at >2% in any interval were shown in Fig. 5. Core Cocos-7 is divided into five pollen zones. The pollen assemblage in Zone-1 (79–61 cm) is dominated by marsh (>60%) and desert taxa (>20%) with very few tree and mangrove taxa. Specifically, most pollen spectra in Zone-1 contain abundant Amaranthaceae (50–70%), an herbaceous plant commonly found in freshwater and brackish marshes (Willard et al., 2001; Yao et al., 2015). In addition, green algae (*Botryococcus*), marine planktons (foraminifera and

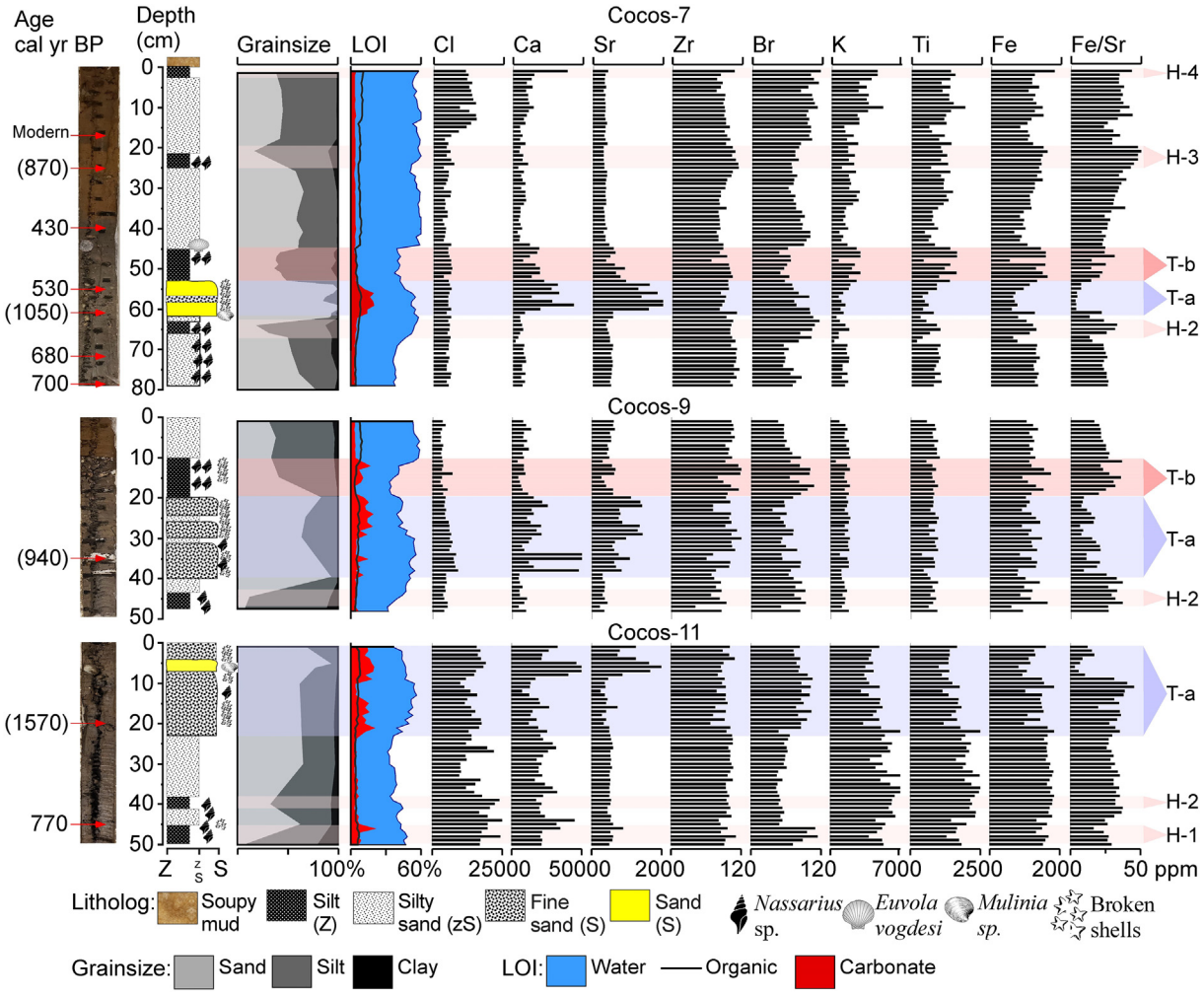

Fig. 4. From left to right: core photograph, litholog, grainsize, LOI, and XRF datasets of cores Cocos-7, Cocos-9, Cocos-11. ^{14}C sample intervals and results are marked by the red arrow. Classification of the grain-size followed the description by Folk (1966). The red and blue shaded zones mark the disturbance events that will be discussed later. (For interpretation of the references to color in this figure legend, the reader is referred to the web version of this article.)

dinoflagellate), desert ironwood (Papilionoideae), beachwort (*Batis* sp.), and aquatic plant (*Ruppia*) are also present in this zone.

Zone-2 (61–45 cm) is characterized by the increase of prolific wind-pollinators, such as red mangrove (*Rhizophora mangle*), pine (*Pinus*), and desert ironwood (Papilionoideae). Concentrations of aquatic taxa (green algae, marine planktons, and *Ruppia*) also increased significantly in this zone, particularly in Zone-2b. The abundant aquatic organisms and rise of red mangrove persisted in Zone-3 (45–37 cm).

Zone 4 (37–15 cm) is characterized by the increase of organic matter (Fig. 4) and the dominance of mangroves, particularly red mangrove. Most intervals in Zone-4 contain >50% of *Rhizophora*, which is indicative of mature red mangrove community (Woodroffe et al., 1985; Behling et al., 2001; Ellison, 2008; Yao and Liu, 2017). Interestingly, red mangrove pollen diminishes abruptly at 25 cm, corresponding to the sandy silt layer with abundant *Nassarius* snails (Figs. 4 & 5).

Zone-5 (15–0 cm) is characterized by a slight decrease in red mangrove pollen and the disappearance of *Botryococcus*, an open-water planktonic algae (Medeanic, 2006; Park et al., 2016; Volkman, 2014). Hence, the disappearance of *Botryococcus* indicates our study area was transformed from a more dynamic environment (Zone-3&4) to an enclosed coastal lagoon (Zone-5), likely caused by the closing of a tidal channel. This transformation also coincides with a significant increase of salinity indicator, Cl (Yao et al., 2020a) in the top 15 cm of core Cocos-7 (Fig. 4).

Core Cocos-9 is divided into Zone-1 (48–40 cm), Zone-2a (40–20 cm), Zone-2b (20–10 cm) and Zone-3 (10–0 cm). Core Cocos-11 is divided into Zone-1 (50–22 cm) and Zone-2a (22–0 cm). The pollen assemblages of the pollen zones in Cocos-9 and Cocos-11 are very similar to the corresponding pollen zones in core Cocos-7 (Fig. 5).

5. Discussion

5.1. Stratigraphic correlation of sediment units in Cocos-7, Cocos-9, and Cocos-11

The stratigraphic units and pollen zones described in Cocos-9 and Cocos-11 can be correlated with those in Cocos-7 (Fig. 6). Using the reddish unit at the top of Cocos-7 (0–40 cm) and Cocos-9 (0–10 cm) as a stratigraphy marker (Figs. 4 & S1), the surface of Cocos-9 (0 cm) corresponds to ~30 cm in Cocos-7. The reddish brown color at the top of these two cores is likely the result of oxidation of ferrous iron in surface sediments where oxygen concentration is higher. Moving into deeper part of the cores, the silt (T-b) and sand layers (T-a), encountered in both cores, are characterized by similar stratigraphic and chemical signatures, as well as almost identical pollen and shell assemblages (Figs. 4 & 5). In particular, the same sand unit (T-a) also occurrs at the top 22 cm of core Cocos-11. Hence, the sand layer in Cocos-7 (53–61) corresponds to those in Cocos-9 (20–40) and Cocos-11 (0–22 cm),

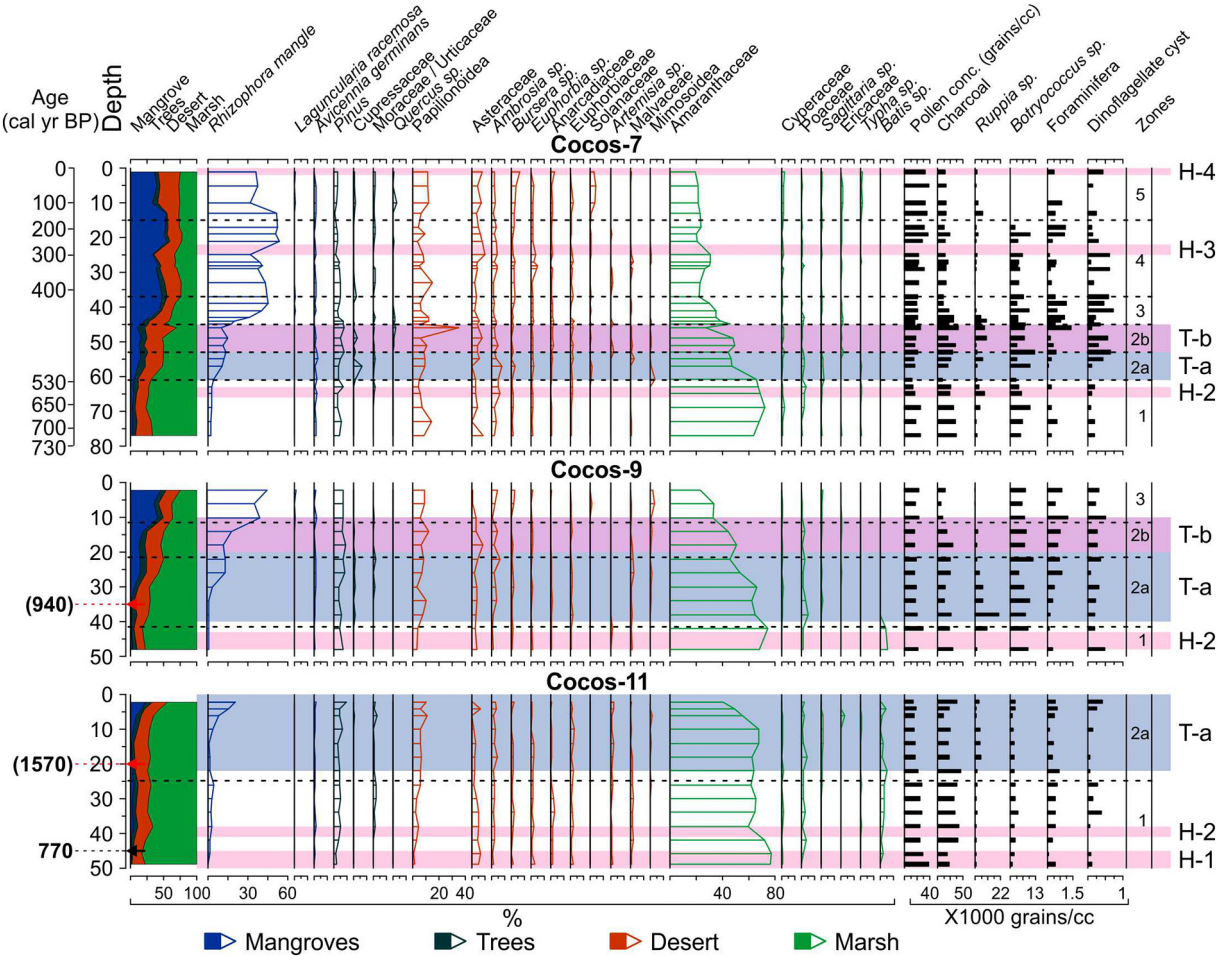

Fig. 5. Pollen results for core Cocos-7, Cocos-9, and Cocos-11. Each vegetation group is marked by a different color and event layers are marked by red and blue shades. The age model for Cocos-7 is generated by *BACON 2.2*. (For interpretation of the references to color in this figure legend, the reader is referred to the web version of this article.)

and silt layers in Cocos-7 (45–53 cm) and Cocos-9 (10–20 cm) correspond with each other (Fig. 6). Similarly, the silt layer (H-2) in Cocos-7 (63–66 cm) corresponds to those in Cocos-9 (43–48 cm), and Cocos-11 (38–41 cm). In addition, two more silt layers (H-3 and H4) are present exclusively in Cocos-7, and another silt layer is present exclusively at the bottom of Cocos-11 (H-1). Fig. 6 summarizes the stratigraphy, LOI, and pollen results of the three cores, and the correlation of the sediment units.

5.2. Sedimentary and geochemical characteristics of hurricane deposits

One of the most distinctive features of the stratigraphic profile of Laguna Los Cocos is the four thin silt layers found in the cores (Fig. 6). Not only do these silt layers share many common physical and chemical characteristics, such as low organic and water content, low concentration of marine elements (e.g., Ca and Sr), and high concentration of terrestrial elements (e.g., Ti and Fe) (Fig. 4), they also resemble the physical and chemical signature of surface samples taken from the fluvial valley (S9-S11) and hillslopes (S12-S14) surrounding the lagoon (Fig. 3). In general, there are three allochthonous endmember sources for lagoonal deposits in Baja California Peninsula: aeolian dust, terrestrially-originated materials, and marine-originated materials (Case et al., 2002), and the latter two endmembers account for the bulk of the sediment profile (Pye, 2015). Typically, terrestrial deposits are generated by landslide (Chagué-Goff et al., 2017) and surface runoff (Yao et al., 2019), whereas tidal activity, storm surge (Wallace et al., 2014; Yao et al., 2020a), and tsunami (McCloskey et al., 2015; Chagué et al., 2020; Ramírez-Herrera et al., 2020) can introduce marine sediments to the lagoon. In the case of Laguna Los Cocos, it is reasonable to assume that earthquake-induced landslides would generate much thicker deposits at occluded environments such as our study site (Fig. 1). Hence, the silt layers are likely fluvial and slope-wash deposits caused by precipitation, particularly heavy precipitation associated with strong tropical storms or hurricanes.

Among instrumental and historical hurricane records in the literature, most studies are focused on storm surge and saltwater intrusion (Liu and Fearn, 1993, 2000; Liu et al., 2008; Donnelly et al., 2001; Brandon et al., 2013; Ercolani et al., 2015). Very few studies have paid attention to evidence of hurricane induced heavy precipitation and flooding (Wang et al., 2019; Yao et al., 2020a), which can cause significant damage to the infrastructure and ecosystem and leave a profound physical and chemical signal in the sediment profile, typically marked by high concentrations of terrestrial runoff indicators (Fe and Ti) (Liu et al., 2014; Yao et al., 2019). In southern Baja California, the majority of the annual precipitation is associated with tropical cyclones (McDonald et al., 2003; Antinao et al., 2016; Antinao and Farfán, 2013). Considering the strong evaporation in an arid desert environment (accumulated annual precipitation of 110 mm/yr) at our study site (SMN, 2020) (Fig. 1), it is likely that slow-moving cyclones carrying a lot of moisture are responsible for forming a deluge on the flood plain and washing the terrestrial sediments downslope into the lagoon. More importantly, Laguna Los Cocos is located in a semi-enclosed bay sheltered by the mountain belts to the west and a small gulf to the east (Fig. 1). Such environmental setting attenuates the physical force of hurricanes and protects Playa Los Cocos from strong storm surges. Thus, the four silt layers (H1 to H4) in the cores were likely formed by

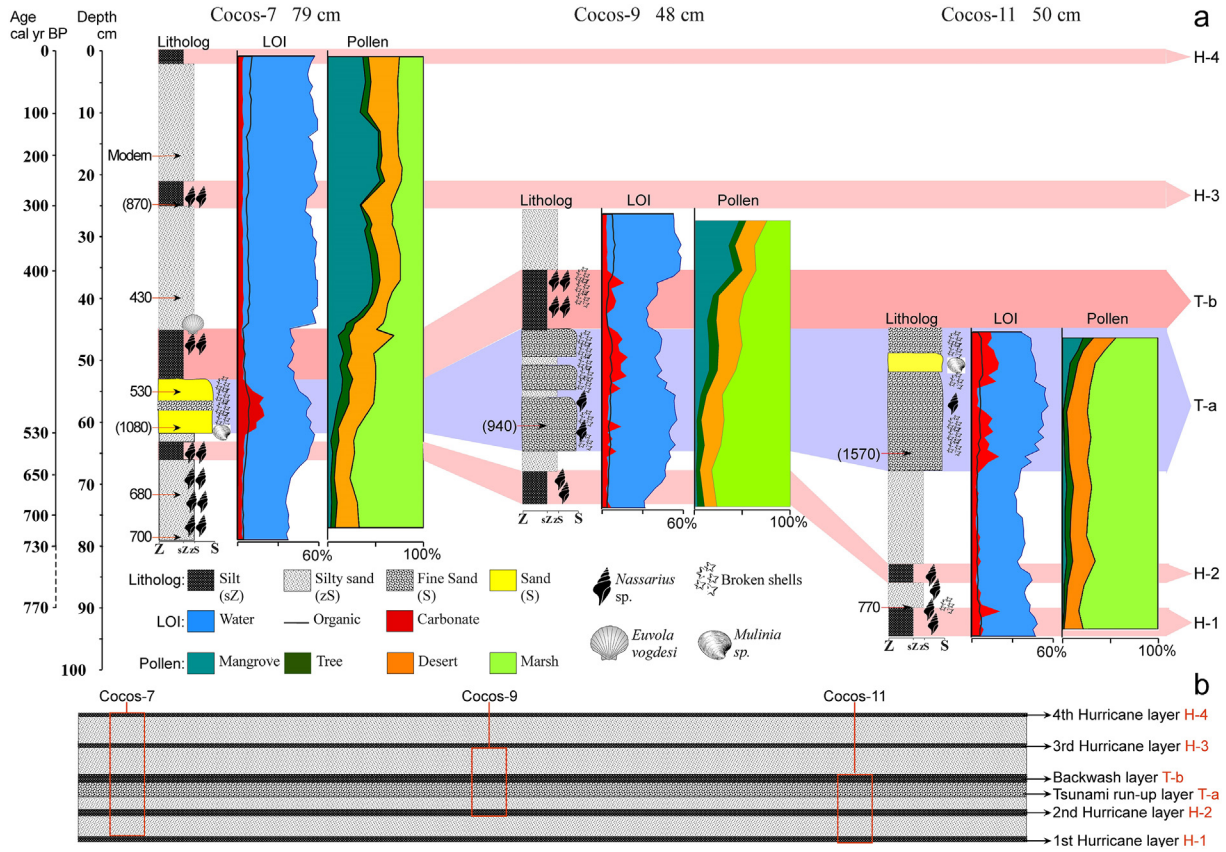

Fig. 6. a) A summary of the proxy records and radiocarbon dates detailing the stratigraphic correlation of cores. Hurricane-generated silt layers (H-1 to H-4) are marked by red shades for visual clarity. Tsunami-generated sand (T-a) and silt (T-b) layers are marked by blue and red shades. Arrows mark the ^{14}C dates (cal yr BP). The age model for Cocos-7 is generated by *BACON 2.2*. The vertical positioning of the cores is based on field notes. b) An illustration of the stratigraphic sequence at the bottom of Laguna Los Cocos. (For interpretation of the references to color in this figure legend, the reader is referred to the web version of this article.)

fluvial and slope-wash processes associated with the passage of slow-moving and wet hurricanes in the past.

In addition, intact shells of *Nassaruis* snails are present in all hurricane layers. *Nassaruis* snails (nassa mud snails) are primarily a deposit-feeder and burrower that actively scavenges on shallow-water and tidal flats (Scheltema, 1964). It is likely that hurricane deposition made the lagoon shallower or the mud flats more extensive, thereby allowing these scavengers to feed in the coring sites where the water was otherwise too deep for these shallow-water burrowers. It is also remarkable that while the fluvial, slope-wash, and lake surface samples have similar grainsize distributions (Fig. 3), hurricane layers in the cores contain a somewhat greater fraction of fine-grained sediments (Fig. 4). We believe that this can be explained by the water-sorting process, whereby the coarser sediments were readily deposited at the foot of the hillslopes or around the edges of the lagoon, and only the fine fractions were deposited at our coring sites toward the center (Zhang et al., 2019, 2020). Moreover, the surrounding vegetation could also act as a filter to prevent the coarser sediments from entering the lagoon.

5.3. Sedimentary and geochemical characteristics of tsunami deposits

The other distinct feature of the stratigraphic profile is the corresponding sand layer (T-a) found in all cores (Fig. 6). This sand layer is characterized by high contents of carbonate and marine elements, low concentrations of terrestrial elements (Fig. 4), and high resemblance to the beach and offshore surface sample groups (Fig. 3). Thus, it is safe to assume a marine origin for this thick sand layer (15–20 cm), which was likely introduced to the lagoon by a major marine intrusion event such as during a strong hurricane or a tsunami. In the case of Playa Los Cocos, we believe this thick sand layer was caused by a paleotsunami, based on several additional pieces of evidence. First, abundant broken shells and intact shells of *Mulinia* sp. (a sea clam found in offshore environment) are present exclusively in the sand layers. This fossil shell assemblage is almost identical to the extant shell assemblages found in nearshore and offshore environments at our study area (Fig. S5 in Supplementary Content). Moreover, large, intact sea shells, especially clams, have been found abundantly in coastal and lagoonal deposits attributed to tsunami events near La Paz, ~320 km south of our study site (McCloskey et al., 2015). Thus, evidence from both the sand layer and the embedded shells point to not only the marine or offshore origin of the deposit, but also a very high-energy mechanism—likely a tsunami—responsible for its transportation and deposition. Second, this sand layer has sharp basal contact with the underlying sediments, implying deposition by an abrupt event (Fig. 4). Third, the physical settings at Playa Los Cocos shelter the lagoon from storm surge (Fig. 1). Most of the tropical cyclones affecting the study area were traveling up the Baja California peninsula from south to north or coming from the Pacific Ocean to the west (Fig. 2). Therefore, they were typically weakened when they made landfall before coming close to the site. In addition, the study site is further protected by a high mountain range in the west, and by the mountainous Concepcion Peninsula across a deep and narrow strait (Bahia Concepcion) in the east (Fig. 1), which further reduces the fetch and hence storm surge height. Furthermore, the physical and chemical characteristics of this sand layer is consistent with those of typical tsunami run-up deposits documented worldwide (Minoura and Nakaya, 1991; Dawson and Stewart, 2007; Goff et al., 2012; McCloskey et al., 2015; Chagué-Goff et al., 2017; Ramírez-Herrera et al., 2020). Therefore, the multi-proxy

dataset indicates that a paleo-tsunami event was recorded in our cores, and it was likely a local tsunami caused by submarine landslide or landside on the east shore of Bahia Concepcion (Fig. 1b), because our study site is sheltered by Bahia Concepcion from large basin-wise tsunami coming from the Gulf of California.

Immediately above the tsunami run-up layers (T-a) in cores Cocos-7 and Cocos-9 is another silt layer (T-b) (Fig. 4). Unlike the other hurricane-generated silt layers (H1-H4), T-b is much thicker and characterized by a mixed physical and chemical signature characteristic of both marine and terrestrial sediments, such as broken shells and finer grainsize. We believe that this thick silt layer is generated by tsunami-triggered backwash. During the tsunami run-up stage, most of the coarser marine sediments (e.g., sand and shells) is dropped out of the water column (Shi et al., 1995; Nanayama and Shigeno, 2006; Dawson and Stewart, 2007), forming the tsunami run-up deposits (T-a) discussed in the previous paragraph (Fig. 6). In Playa Los Cocos, the tsunami run-up must have collected plenty of fluvial and slope-wash sediments from the adjoining landscape. When the tsunami run-up was receding back to the sea, the finer materials containing a mixture of slope-wash sediments (e.g., fine grainsize sediments) and remaining of the marine materials (e.g., broken shells and scallop) gradually deposited on top of the coarser materials (T-a), forming this unique backwash layer (T-b) carrying both marine and terrestrial signals (Figs. 4 and 6).

5.4. The composite ^{14}C age model for Cocos-7, Cocos-9, and Cocos-11

The identification of tsunami and hurricane deposits and close stratigraphic correlation among the cores permits a composite dating scheme for all the disturbance events and zone boundaries (Fig. 6). Two ^{14}C samples taken from the silty sand layers near the bottom of Cocos-7 and Cocos-11 produced similar dates of 700 and 770 cal yr BP (Fig. 6). It is reasonable to infer that the bottom age of Cocos-7 is between 700 and 770 cal yr BP, and the first hurricane layer (H-1) occurred before 770 cal yr BP.

Among the four ^{14}C samples taken from the three hurricane layers, two samples based on bulk sediments and one sample based on seeds yielded anomalously older dates of 1080 (60 cm from Cocos-7), 940 (35 cm from Cocos-9), and 1570 (20 cm from Cocos-11) cal yr BP (Table 1 and Fig. 6). Tsunami and hurricane deposits are essentially a mixture of two fundamentally different sediment sources, autochthonous and allochthonous deposits. The former refers to in-situ deposits, and the latter refers to deposits carried by tsunami run-up or storm surge (Kelsey and Witter, 2020). The bulk sediments and seeds likely represent the allochthonous portion of the tsunami deposits from offshore or nearshore environments, thereby yielding much older dates. The same interpretation also applies to the ^{14}C date from the hurricane layer (25 cm) in Cocos-7 (Fig. 6). However, the leaf sample taken at 55 cm from core Cocos-7 yielded a ^{14}C date of 530 cal yr BP (Table 1), consistent with other valid dates in this core (Figs. 4 & 6). We believe that this sample represents the autochthonous portion of the tsunami deposits, hence a reliable estimate of the calendar age of the tsunami event, since leaf is the optimal sample type for radiocarbon dating. Similar interpretation for radiocarbon dating of tsunami deposits has been reported in previous studies (Ishimura, 2017; Kelsey and Witter, 2020). More importantly, the Bayesian chronology model of Cocos-7 was also in agreement with our interpretation and excluded the two ^{14}C dates based on bulk sediments from the hurricane (25 cm) and tsunami (60 cm) layers (see Fig. S2 in Supplementary Content).

Therefore, based on the composite ^{14}C dating scheme and multi-proxy analysis for Cocos-7, Cocos-9, and Cocos-11, the estimated ages for the four hurricane events are ~770 (H-1), ~600 (H-2), ~280 (H-3), and ~0 (H-4) cal yr BP, and the age of the tsunami event is ~530 (T-a and T-b) cal yr BP (Fig. 6). Among the four inferred hurricane events, three are prehistoric and there are no historical records to corroborate them since the instrumental record from NOAA only documented hurricanes since 1950 CE. The 0 cal yr BP (H-4) event may be Hurricane Olivia of 1967, one of the strongest (category 3) hurricanes that impacted the study area in the historical record (see Section 2.2 above).

5.5. Coastal geomorphological and vegetation changes in response to disturbance events

Overall, the pollen record reveals five vegetation units (Zone-1 to Zone-5) from Cocos-7, three corresponding vegetation units (Zone-1 to Zone-3) from Cocos-9, and one and half corresponding vegetation units (Zone-1 to Zone 2a) from Cocos-11 (Fig. 5). These vegetation units correspond to five stages of vegetation development in response to disturbance events and long-term environmental changes (Fig. 7). To provide a coherent representation of the vegetation and landscape transformation, the three pollen records from Laguna Los Cocos are correlated schematically and displayed in Fig. 7. The age estimation of each stage is primarily based on the Bayesian model of Cocos-7 and the composite ^{14}C dating scheme.

Prior to ~530 cal yr BP, pollen assemblage in Zone-1 (Fig. 5) is consistent with the vegetation composition of a typical coastal saltmarsh in southern Baja California (Case et al., 2002). Such areas were probably dominated by halophytic marsh plants of the family Amaranthaceae (Chenopodiaceae/Amaranthaceae). The consistent appearance of green algae and marine planktons indicates that the area was in close proximity to the intertidal zone, and the abundance of *Nassarius* snails point to a tidal flat. Thus, our record suggests that during the time of Zone-1 (770–530 cal yr BP) the study site was most likely a short-hydroperiod tidal marsh surrounded by drought-tolerant upland plants such as pine, desert ironwood, and other desert plants on the surrounding hillslopes (Fig. 7a). Two hurricanes (*H*-1, *H*-2) affected this site during this time, at ~770 and ~600 cal yr BP. These storms seemed to be detrimental to the halophytic marsh community, as suggested by a decrease in Amaranthaceae pollen above the storm layers, but their ecological impacts seemed to be limited.

This coastal saltmarsh landscape persisted until ~530 cal yr BP when the tsunami hit Playa Los Cocos. The pollen assemblages in the tsunami run-up layer (Zone-2a) is characterized by a sharp decrease in the locally-derived Amaranthaceae and an increase in *Rhizophora*, which was hitherto absent or rare locally at the study site but was probably present in other suitable coastal habitats around Bahia Concepcion and, as a corollary, in the offshore sediments (Fig. 5). This pollen signature is consistent with the phenomenon documented by previous studies that offshore or marine sediments contain a more regional pollen assemblage than the in-situ terrestrial sediments (Chmura and Liu, 1990; Chmura et al., 1999; Yao and Liu, 2018). The pollen assemblage in the tsunami backwash layer (Zone-2b) contains more desert taxa found on the hillslopes (e.g., Asteraceae, Papillionoideae), especially in Cocos-7. This pollen signature is also consistent with the sedimentary process of the tsunami-trigger backwash. The multi-proxy evidence from Zone-2, the tsunami event deposit, suggests that a sand barrier was formed in front of the coastal saltmarsh, eventually transforming the bay-mouth wetland into a backbarrier lagoon (Fig. 7b). During the tsunami run-up, large volumes of materials were eroded from the subtidal and intertidal zone and deposited on the coastal plain and in the saltmarsh (Dawson and Stewart, 2007), generating a beach barrier, trapping the seawater, and creating a lagoon behind it (Evans et al., 2011). Accordingly, the backbarrier lagoon preserves not only the landward-directed run-up deposit (T-a) but also the seaward-directed backwash deposit (T-b). Such barrier lakes created by the impounding of coastal water due to tsunami or other tectonic activities have been documented worldwide, and it may persist for thousands of years (Jansen, 2012).

The backbarrier lagoon persisted through Zone-3 (~530–400 cal yr BP) (Fig. 5). During this early phase of development, the lagoon was fairly open with active tidal connections to the sea, as evidenced by the great abundance of foraminifera tests and dinoflagellates. The

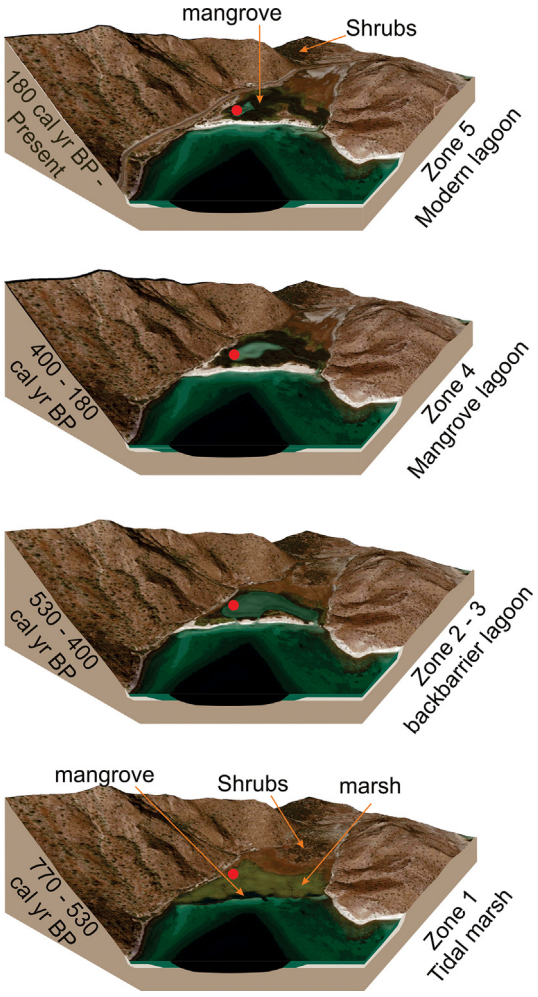

Fig. 7. Graphic simulation of the geomorphology and vegetation development of Playa Los Cocos associated with disturbance events and environmental change during the late Holocene, based on proxy data and modern terrain and vegetation. Red dot marks the study site. Mangroves and marshes are marked in darker-green and lighter-green patches around the lagoon. (For interpretation of the references to color in this figure legend, the reader is referred to the web version of this article.)

lagoonal environment must have provided favorable habitats for red mangroves, which rapidly colonized the littoral zones of the lagoon with expanding populations (Fig. 7b).

Mangroves continued to proliferate and progressively replaced the beach and marsh taxa in Zone-4 (~400–180 cal yr BP) (Fig. 7c). *Rhizophora* generally accounts for >50% of the pollen assemblage (Fig. 5), indicating a well-established red mangrove forest around the lagoon (Behling et al., 2001; Ellison, 2008; Yao et al., 2015; Yao and Liu, 2017). As the sand barrier continued to grow and stabilize, the lagoon became more isolated from the sea, as indicated by the notable decrease in foraminifera tests and dinoflagellates in this zone. The lagoon, while less tidally connected, also became shallower due to sediment infilling, as suggested by the disappearance of aquatic plant (*Ruppia*) and a decrease of green algae (*Botryococcus*) (Fig. 5). The expansion of mangrove and increase of organic matter in Zone-3 and Zone-4 suggest an increase in mangrove peat accumulation after the tsunami event (Figs. 4 & 5). It has been documented that that major coastal disturbance events, such as hurricanes and storm surges, can bring phosphorus and nitrogen from offshore sediments to fertilize mangrove forests, and the additional nutrients could accelerate mangrove expansion (Yao and Liu, 2017, 2018; Yao et al., 2015) and mangrove peat accumulation (Castañeda-Moya et al., 2013, 2020). Since tsunami and hurricane deposits share similar physical and chemical characteristics (Ramírez-Herrera et al., 2012; Chagué-Goff et al., 2017), it is reasonable to assume that the tsunami deposits also fertilized the mangrove forest in Playa Los Cocos and facilitated its rapid expansion. In addition, tsunami waves could have transported propagules of *Rhizophora* from red mangrove colonies around other coastal areas in Bahia Concepcion to our study site, where mangroves were hitherto absent. In mangrove literature, sea-level rise has been reported to be the main driver for mangrove peat accumulation in several desert inlets along the coasts of Baja California (Ezcurra et al., 2016) and in other regions across the globe (McKee et al., 2007; Ellison, 2008; López-Medellín et al., 2011). This study documents that tsunami events may also be beneficial for the spread and proliferation of mangroves in a desert environment by possibly facilitating propagule dispersal, creating suitable habitats, and fertilizing the substrate. It is also remarkable that the site was impacted by another hurricane (H-3) around ~280 cal yr BP (Fig. 4). The pollen data suggest that this storm event might have caused significant mortality of red mangrove around the site but its population recovered quickly and might even have benefited from this disturbance event, as indicated by a distinct increase in *Rhizophora* pollen above the storm layer (Fig. 5). The halophytic marsh community also seemed to be adversely affected by this storm event.

Finally, since ~180 cal yr BP (Zone-5), red mangrove has continued to dominate the vegetation community around Playa Los Cocos, albeit at lower abundance than before (Fig. 7d). The reduced mangrove population was probably due to increased human activities, which started in the late 17th century when the first Spanish mission was founded in Loreto and culminated in the 1830s (Case et al., 2002). In a barren desert terrain such as south Baja California, mangrove wood is among the few natural resources that can be used for fuel or other human consumptions. During this period the lagoon probably continued to shrink in size as a result of silting, as suggested by the disappearance of the open-water planktonic algae *Botryococcus* (Fig. 5). Thus, the coring site became increasingly isolated from the sea and became a backbarrier lake, as reflected by the significant reduction in the frequencies of foraminifera tests and dinoflagellates in this zone. While very limited tidal connection is still being maintained to-date by a small inactive channel running to the north and northeast of the lake, the lake has received most of its sediment and nutrient input from terrestrial sources and might have become hypersaline during drier periods, which is registered by a concomitant increase in Ti, Fe, K, and the salinity indicator Cl in the XRF record (Fig. 4).

6. Conclusions

This study provides the first paleo-hurricane record and a hitherto undocumented paleo-tsunami event at ~530 cal yr BP from southern Baja California, Mexico. The multi-proxy sedimentary record documents four hurricane events at ~770 (H-1), ~600 (H-2), ~280 (H-3), and ~0 (H-4) cal yr BP, and one tsunami event at ~530 (T-a and T-b) cal yr BP (Fig. 6). The hurricane deposits were preserved in the form of fluvial and slope-wash deposits and characterized by low organic and water contents, low concentrations of marine elements (e.g., Ca and Sr), and high concentrations of terrestrial elements (e.g., Ti and Fe) (Fig. 4). This study also documents the physical, chemical, and biological characteristics of a tsunami deposit, including both the run-up and backwash facies. The tsunami run-up deposits are characterized by abundant broken and intact sea shells, high contents of carbonate and marine elements, low concentrations of terrestrial elements, and sharp basal contact with the underlying sediments. In contrast, the tsunami backwash deposits are characterized by a mixed physical and chemical signature resembling both marine and terrestrial sediments.

By integrating pollen data with sedimentary and geochemical evidence of paleo-tsunami and paleo-hurricane events, this study provides a rare dataset that documents the post-disturbance geomorphic and ecosystem changes at a coastal lagoonal site in an arid landscape. The multi-proxy dataset documents five stages of vegetation and landscape transformation in response to disturbance events and environmental

changes during the last millennium (Fig. 7). Prior to ~530 cal yr BP, Playa Los Cocos was occupied by a short-hydroperiod tidal saltmarsh bounded by drought-tolerant species on the surrounding hillslopes (Fig. 7a). The ~530 cal yr BP tsunami event deposited a sand barrier in front of the saltmarsh, creating a backbarrier lagoon that was initially tidally open to the sea (Fig. 7b). Mangroves were previously absent from the site but the tsunami waves probably brought mangrove propagules in from other coastal localities, and the lagoonal environment and substrates also provided suitable habitats for red mangroves to proliferate (Fig. 7b). Once established, red mangrove populations rapidly expanded and became the dominant species around the backbarrier lagoon after ~400 cal yr BP (Fig. 7c). Hurricane disturbances also seemed to have similar beneficial effects on mangrove populations as tsunamis in this arid coastal lagoonal environment. Mangrove abundance was somewhat diminished during the past two centuries due to human activities. Meanwhile, the lagoon has shrunk in size due to silting, especially in the northern and eastern sides, and it became increasingly isolated from marine influences (Fig. 7d). The modern shallow, saline backbarrier lake surrounded by mangroves was formed after ~180 cal yr BP as a result of these long-term coastal morphodynamic and ecological processes punctuated by disturbance events caused by a tsunami, multiple hurricanes, and human activities.

CRediT authorship contribution statement

Dr. Qiang Yao contributed to field work, conceptual and graphic design, writing, editing, and all laboratory analyses of this study.

Dr. Kam-biu Liu contributed to field work, conceptual design, and editing of this manuscript.

Dr. Yijing Wu contributed to short-lived isotope dating of the cores and the writing of the manuscript.

Dr. Alejandro Antonio Aragón-Moreno contributed to field work, conceptual and graphic, and pollen analyses of this study.

Ms. Erika Rodrigues contributed to grainsize analysis of this study.

Dr. Marcelo Cohen contributed to grainsize analysis and editing of the manuscript.

Ms. Adriana V. de Souza contributed to the graphic design of Fig. 7 and the Graphic Abstract.

Dr. Luis M. Farfán contributed to field work and editing of this manuscript.

Dr. Jose Luis Antinao contributed to field work and editing of this manuscript.

Declaration of competing interest

The authors declare that they have no known competing financial interests or personal relationships that could have appeared to influence the work reported in this paper.

Acknowledgements

This research was supported by grants from the U.S. National Science Foundation (Grant # EAR-1745741) and State Key Laboratory of Marine Geology (Grant # MGK-1911). We thank Dr. Junghyung Ryu for his assistance in fieldwork.

Data availability

All of the datasets produced in this article will be stored at the Neotoma Paleoecology Database (https://www.neotomadb.org) upon publication and accessible to the public for free.

Appendix A. Supplementary data

Supplementary data to this article can be found online at https://doi.org/10.1016/j.scitotenv.2021.149011.

References

Antinao, J.L., Farfán, L.M., 2013. Occurrence of landslides during the approach of tropical cyclone Juliette (2001) into Baja California Sur, Mexico. Atmósfera 26 (2), 183–208.
Antinao, J.L., McDonald, E., 2011. Three hundred years of hurricanes in Baja California from documentary sources: Implications for sediment flux and landscape evolution in the peninsula. Annual Conference. American Association of Geographers, Seattle, p. 56.
Antinao, J.L., McDonald, E., Rhodes, E.J., Brown, N., Barrera, W., Gosse, J.C., Zimmermann, S., 2016. Late Pleistocene-Holocene alluvial stratigraphy of southern Baja California, Mexico. Quat. Sci. Rev. 146, 161–181.
Aragón-Moreno, A.A., Islebe, G.A., Torrescano-Valle, N., 2012. A ~3800-yr, high-resolution record of vegetation and climate change on the north coast of the Yucatan Peninsula. Rev. Palaeobot. Palynol. 178, 35–42.
Aragón-Moreno, A.A., Islebe, G.A., Roy, P.D., Torrescano-Valle, N., Mueller, A.D., 2018. Climate forcings on vegetation of the southeastern Yucatán Peninsula (Mexico) during the middle to late Holocene. Palaeogeogr. Palaeoclimatol. Palaeoecol. 495, 21–226.
Arianoutsou, M., Leone, V., Moya, D., Lovreglio, R., Delipetrou, P., de las Heras, J., 2012. Management of threatened, high conservation value, forest hotspots under changing fire regimes. Post-fire Management and Restoration of Southern European Forests. Springer, Dordrecht, pp. 257–291.
Bedsworth, L., Cayan, D., Franco, G., Fisher, L., Ziaja, S., 2018. Statewide Summary Report. California's Fourth Climate Change Assessment. (No. SUMCCCA4-2018 - 013). California Governor's Office of Planning and Research, Scripps Institution of Oceanography, California Energy Commission, California Public Utilities Commission.
Behling, H., Cohen, M.C.L., Lara, R.J., 2001. Studies on Holocene mangrove ecosystem dynamics of the Bragança Peninsula in north-eastern Pará, Brazil. Palaeogeogr. Palaeoclimatol. Palaeoecol. 167, 225–242.
Blaauw, M., 2010. Methods and code for 'classical' age-modelling of radiocarbon sequences. Quat. Geochronol. 5, 512–518.
Brandon, C.M., Woodruff, J.D., Lane, D.P., Donnelly, J.P., 2013. Tropical cyclone wind speed constraints from resultant storm surge deposition: a 2500-year reconstruction of hurricane activity from St. Marks, FL. Geochem. Geophys. Geosyst. 14, 2993–3008.
Bregy, J.C., Wallace, D.J., Minzoni, R.T., Cruz, V.J., 2018. 2500-year paleotempestological record of intense storms for the northern Gulf of Mexico, United States. Mar. Geol. 396, 26–42.
Case, T.J., Cody, M.L., Ezcurra, E. (Eds.), 2002. A New Island Biogeography of the Sea of Cortés. Oxford University Press.
Castañeda-Moya, E., Twilley, R.R., Rivera-Monroy, V.H., 2013. Allocation of biomass and net primary productivity of mangrove forests along environmental gradients in the Florida Coastal Everglades, USA. For. Ecol. Manag. 307, 226–241.
Castañeda-Moya, E., Rivera-Monroy, V.H., Chambers, R.M., Zhao, X., Lamb-Wotton, L., Gorsky, A., 2020. Hurricanes fertilize mangrove forests in the Gulf of Mexico (Florida Everglades, USA). Proc. Natl. Acad. Sci. 117 (9), 4831–4841.
Castro, R.R., Stock, J.M., Hauksson, E., Clayton, R.W., 2017. Active tectonics in the Gulf of California and seismicity (M> 3.0) for the period 2002–2014. Tectonophysics 719, 4–16.
Chagué, C., Cope, J., Kilroy, C., Jacobsen, G., Zawadzki, A., Wong, H., 2020. A 7300-year record of environmental changes in a coastal wetland (Moawhitu), New Zealand, and evidence for catastrophic overwash (tsunami?). Sediment. Geol. 407, 105–746.
Chagué-Goff, C., Schneider, J.L., Goff, J.R., Dominey-Howes, D., Strotz, L., 2011. Expanding the proxy toolkit to help identify past events—lessons from the 2004 Indian Ocean Tsunami and the 2009 South Pacific Tsunami. Earth Sci. Rev. 107 (1–2), 107–122.
Chagué-Goff, C., Szczuciński, W., Shinozaki, T., 2017. Applications of geochemistry in tsunami research: a review. Earth Sci. Rev. 165, 203–244.
Chmura, G.L., Liu, K.B., 1990. Pollen in the lower Mississippi River. Rev. Palaeobot. Palynol. 64 (1–4), 253–261.
Chmura, G.L., Smirnov, A., Campbell, I.D., 1999. Pollen transport through distributaries and depositional patterns in coastal waters. Palaeogeogr. Palaeoclimatol. Palaeoecol. 149 (1–4), 257–270.
Dawson, A.G., 1994. Geomorphological processes associated with tsunami runup and backwash. Geomorphology 10, 83–94.
Dawson, A.G., Shi, S., 2000. Tsunami deposits. Pure Appl. Geophys. 157 (6–8), 875–897.
Dawson, A.G., Stewart, I., 2007. Tsunami deposits in the geological record. Sediment. Geol. 200 (3–4), 166–183.
Dean, W.E., 1974. Determination of carbonate and organic matter in calcareous sediments and sedimentary rocks by loss on ignition; comparison with other methods. J. Sediment. Res. 44 (1), 242–248.
Donnelly, J.P., Roll, S., Wengren, M., Butler, J., Lederer, R., Webb, T., 2001. Sedimentary evidence of intense hurricane strikes from New Jersey. Geology 29 (7), 615–618.
Ellison, J.C., 2008. Long-term retrospection on mangrove development using sediment cores and pollen analysis: a review. Aquat. Bot. 89 (2), 93–104.
Engel, M., Pilarczyk, J., May, S.M., Brill, D., Garrett, E., 2020. Geological Records of Tsunamis and Other Extreme Waves. Elsevier.
Ercolani, C., Muller, J., Collins, J., Savarese, M., Squiccimara, L., 2015. Intense southwest Florida hurricane landfalls over the past 1000 years. Quat. Sci. Rev. 126, 17–25.
Evans, S.G., Hermanns, R.L., Strom, A., Scarascia-Mugnozza, G., 2011. Natural and Artificial Rockslide Dams. vol. 133. Springer Science & Business Media.
Ezcurra, P., Ezcurra, E., Garcillán, P.P., Costa, M.T., Aburto-Oropeza, O., 2016. Coastal landforms and accumulation of mangrove peat increase carbon sequestration and storage. Proc. Natl. Acad. Sci. 113 (16), 4404–4409.
Farreras, S.F., Sanchez, A.J., 1991. The tsunami threat on the Mexican west coast: a historical analysis and recommendations for hazard mitigation. Nat. Hazards 4 (2–3), 301–316.

Figueroa-Rangel, B.L., Olvera-Vargas, M., Vázquez-López, J.M., Willis, K.J., Lozano-García, S., 2016. Modern and fossil pollen assemblages reveal forest taxonomic changes in the Mexican subtropics during the last 1300 years. Rev. Palaeobot. Palynol. 231, 1–13.
Folk, R.L., 1966. A review of grain-size parameters. Sedimentology 6 (2), 73–93.
Glover, K.C., Chaney, A., Kirby, M.E., Patterson, W.P., MacDonald, G.M., 2020. Southern California vegetation, wildfire, and erosion had nonlinear responses to climatic forcing during marine isotope stages 5-2 (120–15 ka). Palaeogeogr. Palaeoclimatol. 35, e2019PA003628.
Goff, J., Chagué-Goff, C., Nichol, S., Jaffe, B., Dominey-Howes, D., 2012. Progress in palaeotsunami research. Sediment. Geol. 243, 70–88.
Goff, J., Witter, R., Terry, J., Spiske, M., 2020. Palaeotsunamis in the Sino-Pacific region. Earth Sci. Rev. 103–352.
Gonzalez-Yajimovich, O.E., Gorsline, D.S., Douglas, R.G., 2007. Frequency and sources of basin floor turbidites in Alfonso Basin, Gulf of California, Mexico: products of slope failures. Sediment. Geol. 199 (1–2), 91–105.
Gorelick, N., Hancher, M., Dixon, M., Ilyushchenko, S., Thau, D., Moore, R., 2017. Google earth engine: planetary-scale geospatial analysis for everyone. Remote Sens. Environ. 202, 18–27. https://doi.org/10.1016/j.rse.2017.06.031.
Haug, G.H., Hughen, K.A., Sigman, D.M., Peterson, L.C., Röhl, U., 2001. Southward migration of the intertropical convergence zone through the Holocene. Science 293 (5533), 1304–1308.
Horton, B., Engelhart, S.E., Kemp, A.C., Sawai, Y., 2013. Microfossils in tidal settings as indicators of sea-level change, paleoearthquakes, tsunamis, and tropical cyclones. Treatise on Geomorphology. Elsevier Inc, pp. 292–314.
Ishimura, D., 2017. Re-examination of the age of historical and paleo-tsunami deposits at Koyadori on the Sanriku Coast, Northeast Japan. Geosci. Lett. 4 (1), 11.
Jansen, R.B., 2012. Advanced Dam Engineering for Design, Construction, and Rehabilitation. Springer Science & Business Media.
Kelsey, H.M., Witter, R.C., 2020. Radiocarbon dating of tsunami and storm deposits. In: Engel, M., Pilarczyk, J., May, S.M., Brill, D., Garrett, E. (Eds.), Geological Records of Tsunamis and Other Extreme Waves. Elsevier, pp. 663–685.
Kortekaas, S., Dawson, A.G., 2007. Distinguishing tsunami and storm deposits: an example from Martinhal, SW Portugal. Sediment. Geol. 200 (3–4), 208–221.
Liu, K.B., 2004. Paleotempestology: principles, methods, and examples from Gulf Coast lake sediments. Hurricanes and Typhoons: Past, Present, and Future, pp. 13–57.
Liu, K.B., Fearn, M.L., 1993. Lake-sediment record of late Holocene hurricane activities from coastal Alabama. Geology 21 (9), 793–796.
Liu, K.B., Fearn, M.L., 2000. Reconstruction of prehistoric landfall frequencies of catastrophic hurricanes in northwestern Florida from lake sediment records. Quat. Res. 54 (2), 238–245.
Liu, K.B., Lu, H., Shen, C., 2008. A 1200-year proxy record of hurricanes and fires from the Gulf of Mexico coast: testing the hypothesis of hurricane–fire interactions. Quat. Res. 69 (1), 29–41.
Liu, K.B., McCloskey, T.A., Ortego, S., Maiti, K., 2014. Sedimentary signature of hurricane Isaac in a *Taxodium* swamp on the western margin of Lake Pontchartrain, Louisiana, USA. Proceedings of the International Association of Hydrological Sciences. 367, pp. 421–428.
López-Medellín, X., Ezcurra, E., González Abraham, C., Hak, J., Santiago, L.S., Sickman, J.O., 2011. Oceanographic anomalies and sea-level rise drive mangroves in land in the Pacific coast of Mexico. J. Veg. Sci. 22 (1), 143–151.
Martínez-López, A., Flores-Castillo, O.D.L.Á., Saldívar-Lucio, R., Escobedo-Urías, D.C., Verdugo-Díaz, G., Pérez-Cruz, L., Albañez-Lucero, M., Acevedo-Acosta, J.D., 2019. Paleoclimate of the Gulf of California (Northwestern Mexico) during the last 2000 years. The Holocene and Anthropocene Environmental History of Mexico. Springer, Cham, pp. 7–38.
McCloskey, T.A., Bianchette, T.A., Liu, K.B., 2015. Geological and sedimentological evidence of a large tsunami occurring~ 1100 year BP from a small coastal lake along the Bay of La Paz in Baja California Sur, Mexico. J. Mar. Sci. Eng. 3 (4), 1544–1567.
McCloskey, T.A., Smith, C.G., Liu, K.B., Marot, M., Haller, C., 2018. How could a freshwater swamp produce a chemical signature characteristic of a saltmarsh? ACS Earth Space Chem. 2 (1), 9–20.
McDonald, E.V., McFadden, L.D., Wells, S.G., Enzel, Y., Lancaster, N., 2003. Regional response of alluvial fans to the Pleistocene-Holocene climatic transition, Mojave Desert, California. Geol. Soc. Am. Spec. Pap. 189–206.
McKee, K.L., Cahoon, D.R., Feller, I.C., 2007. Caribbean mangroves adjust to rising sea level through biotic controls on change in soil elevation. Glob. Ecol. Biogeogr. 16 (5), 545–556.
Medeanic, S., 2006. Freshwater algal palynomorph records from Holocene deposits in the coastal plain of Rio Grande do Sul, Brazil. Rev. Palaeobot. Palynol. 141 (1–2), 83–101.
Minoura, K., Nakaya, S., 1991. Traces of tsunami preserved in inter-tidal lacustrine and marsh deposits: some examples from northeast Japan. J. Geol. 99 (2), 265–287.
Minoura, K., Imamura, F., Sugawara, D., Kono, Y., Iwashita, T., 2001. The 869 Jogan tsunami deposit and recurrence interval of large-scale tsunami on the Pacific coast of northeast Japan. J. Nat. Disaster Sci. 23 (2), 83–88.
Morton, R.A., Gelfenbaum, G., Jaffe, B.E., 2007. Physical criteria for distinguishing sandy tsunami and storm deposits using modern examples. Sediment. Geol. 200 (3–4), 184–207.
Nanayama, F., Shigeno, K., 2006. Inflow and outflow facies from the 1993 tsunami in southwest Hokkaido. Sediment. Geol. 187 (3-4), 139–158.
National Geophysical Data Center/World Data Service (NGDC/ WDS), 2017. NCEI/WDS Global Historical Tsunami Database. NOAA National Centers for Environmental Information. https://doi.org/10.7289/v5pn93h7.
National Hurricane Center (NHC), 2015. 2014 Eastern Pacific hurricane season. Retrieved February 26, 2020 from. https://www.nhc.noaa.gov/data/tcr/summary_epac_2014.pdf.
NOAA Historical Hurricane Tracks, 2020. Retrieved Febuary 26. from. https://oceanservice.noaa.gov/news/historical-hurricanes/.
Páez-Osuna, F., Sanchez-Cabeza, J.A., Ruiz-Fernández, A.C., Alonso-Rodríguez, R., Piñón-Gimate, A., Cardoso-Mohedano, J.G., Flores-Verdugo, F.J., Carballo, J.L., Cisneros-Mata, M.A., Álvarez-Borrego, S., 2016. Environmental status of the Gulf of California: a review of responses to climate change and climate variability. Earth Sci. Rev. 162, 253–268.
Park, J., Shin, Y.H., Byrne, R., 2016. Late-Holocene vegetation and climate change in Jeju Island, Korea and its implications for ENSO influences. Quat. Sci. Rev. 153, 40–50.
Pérez-Cruz, L., 2006. Climate and ocean variability during the middle and late Holocene recorded in laminated sediments from Alfonso Basin, Gulf of California, Mexico. Quat. Res. 65 (3), 401–410.
Pérez-Cruz, L., 2013. Hydrological changes and paleoproductivity in the Gulf of California during middle and late Holocene and their relationship with ITCZ and North American Monsoon variability. Quat. Res. 79 (2), 138–151.
Peters, R., Jaffe, B., 2010. Identification of tsunami deposits in the geologic record; developing criteria using recent tsunami deposits. U.S. Geol. Surv. Open File Rep. 1239 (2010), 39.
Pye, K., 2015. Aeolian dust and dust deposits. Elsevier.
Ramirez-Herrera, M.T., Cundy, A., Kostoglodov, V., Carranza-Edwards, A., Morales, E., Metcalfe, S., 2007. Sedimentary record of Late-Holocene relative sea-level change and tectonic deformation from the Guerrero Seismic Gap, Mexican Pacific Coast. The Holocene 17 (8), 1211–1220.
Ramírez-Herrera, M.T., Lagos, M., Hutchinson, I., Kostoglodov, V., Machain, M.L., Caballero, M., Goguitchaichvili, A., Aguilar, B., Chagué-Goff, C., Goff, J., Ruiz-Fernández, A.C., 2012. Extreme wave deposits on the Pacific coast of Mexico: tsunamis or storms? -a multi-proxy approach. Geomorphology 139, 360–371.
Ramírez-Herrera, M.T., Corona, N., Castillo-Aja, R., 2019. Revealing the source of the 27 August 1810 Loreto, Baja California, tsunami from historical evidence and numerical modelling. Pure Appl. Geophys. 176 (7), 2951–2967.
Ramírez-Herrera, M.T., Corona, N., Cerny, J., Castillo-Aja, R., Melgar, D., Lagos, M., Goguitchaichvili, A., Machain, M.L., Vazquez-Caamal, M.L., Ortuño, M., Caballero, M., 2020. Sand deposits reveal great earthquakes and tsunamis at Mexican Pacific Coast. Sci. Rep. 10 (1), 1–10.
Scheltema, R.S., 1964. Feeding habits and growth in the mud-snail Nassarius obsoletus. Chesap. Sci. 5 (4), 161–166.
Seager, R., Osborn, T.J., Kushnir, Y., Simpson, I.R., Nakamura, J., Liu, H., 2019. Climate variability and change of Mediterranean-type climates. J. Clim. 32 (10), 2887–2915.
Sedlock, R.L., 2003. Geology and tectonics of the Baja California peninsula and adjacent areas. Geol. Soc. Am. Spec. Pap. 1–42.
Servicio Meteorológico Nacional (SMN), 2020. Raingauge records are from Mexico's Servicio Meteorológico Nacional (SMN) historical archive of daily observations. Retrieved March 20, from. https://smn.conagua.gob.mx/tools/RESOURCES/Diarios/3038.txt.
Shi, S., Dawson, A.G., Smith, D.E., 1995. Coastal sedimentation associated with the December 12th, 1992 tsunami in Flores, Indonesia. Tsunamis: 1992–1994. Birkhäuser Basel, pp. 525–536.
Stock, J.M., Hodges, K.V., 1989. Pre-Pliocene extension around the Gulf of California and the transfer of Baja California to the Pacific plate. Tectonics 8 (1), 99–115.
Stuiver, M., Reimer, P.J., Reimer, R., 2020. CALIB radiocarbon Calibration 7.1 [WWW document]. Calib 7.1 URL. http://calib.org/calib/calib.html (accessed 1.31.20).
Suter, M., 2018. The historical seismicity of the Loreto Region, Baja California Peninsula, Mexico (1684–1878). Seismol. Res. Lett. 89 (1), 202–209.
Tuttle, M.P., Ruffman, A., Anderson, T., Jeter, H., 2004. Distinguishing tsunami from storm deposits in eastern North America: the 1929 Grand Banks tsunami versus the 1991 Halloween storm. Seismol. Res. Lett. 75 (1), 117–131.
Underwood, E.C., Viers, J.H., Klausmeyer, K.R., Cox, R.L., Shaw, M.R., 2009. Threats and biodiversity in the Mediterranean biome. Divers. Distrib. 15, 188–197.
Van Soelen, E.E., Brooks, G.R., Larson, R.A., Sinninghe Damsté, J.S., Reichart, G.J., 2012. Mid- to Late-Holocene coastal environmental changes in southwest Florida, USA. The Holocene 22 (8), 929–938.
Vargas-Sánchez, R.D., Peñalba-Garmendia, M.C., Sánchez-Escalante, J.J., Torrescano-Urrutia, G.R., Sánchez-Escalante, A., 2016. Pollen profile of propolis produced on the eastern edge of the Sonoran Desert in central Sonora, Mexico. Acta Bot. Mex. (114), 69–85.
Volkman, J.K., 2014. Acyclic isoprenoid biomarkers and evolution of biosynthetic pathways in green microalgae of the genus Botryococcus. Org. Geochem. 75, 36–47.
Wallace, D.J., Woodruff, J.D., Anderson, J.B., Donnelly, J.P., 2014. Palaeohurricane reconstructions from sedimentary archives along the Gulf of Mexico, Caribbean Sea and western North Atlantic Ocean margins. Geol. Soc. Lond., Spec. Publ. 388 (1), 481–501.
Wang, L., Bianchette, T.A., Liu, K.B., 2019. Diatom evidence of a paleohurricane-induced coastal flooding event in Weeks Bay, Alabama, USA. J. Coast. Res. 35 (3), 499–508.
Willard, D.A., Weimer, L.M., Riegel, W.L., 2001. Pollen assemblages as paleoenvironmental proxies in the Florida Everglades. Rev. Palaeobot. Palynol. 113 (4), 13–235 2.
Woodroffe, C.D., Thom, B.G., Chappell, J., 1985. Development of widespread mangrove swamps in mid-Holocene times in northern Australia. Nature 317 (6039), 711–713.
Woodruff, J.D., Donnelly, J.P., Mohrig, D., Geyer, W.R., 2008. Reconstructing relative flooding intensities responsible for hurricane-induced deposits from Laguna Playa Grande, Vieques, Puerto Rico. Geology 36 (5), 391–394.
Yao, Q., Liu, K.B., 2017. Dynamics of marsh-mangrove ecotone since the mid-Holocene: a palynological study of mangrove encroachment and sea level rise in the Shark River Estuary, Florida. PLoS One 12, e0173670.
Yao, Q., Liu, K.B., 2018. Changes in modern pollen assemblages and soil geochemistry along coastal environmental gradients in the Everglades of South Florida. Front. Ecol. Evol. 5, 178. https://doi.org/10.3389/fevo.2017.00178.

Yao, Q., Liu, K.B., Platt, W.J., Rivera-Monroy, V.H., 2015. Palynological reconstruction of environmental changes in coastal wetlands of the Florida Everglades since the mid-Holocene. Quat. Res. 83, 449–458.
Yao, Q., Liu, K.B., Ryu, J., 2018. Multi-proxy characterization of hurricanes Rita and Ike storm deposits in the Rockefeller wildlife refuge, southwestern Louisiana. J. Coast. Res. 85 (SI), 841–845.
Yao, Q., Liu, K.B., Williams, H., Joshi, S., Bianchette, T.A., Ryu, J., Dietz, M., 2019. Hurricane Harvey storm sedimentation in the San Bernard National Wildlife Refuge, Texas: fluvial versus storm surge deposition. Estuar. Coasts 43 (5), 971–983.
Yao, Q., Liu, K.B., Aragón-Moreno, A.A., Rodrigues, E., Xu, Y.J., Lam, N.S., 2020. A 5200-year paleoecological and geochemical record of coastal environmental changes and shoreline fluctuations in southwestern Louisiana: implications for coastal sustainability. Geomorphology 107–284.
Yao, Q., Liu, K.B., Rodrigues, E., Bianchette, T., Aragón-Moreno, A.A., Zhang, Z.A., 2020a. Geochemical record of Late - Holocene hurricane events from the Florida Everglades. Water Resour. Res. 56 (8), e2019WR026857.
Zhang, Z., Yao, Q., Bianchette, T.A., Liu, K.B., Wang, G., 2019. A multi-proxy quantitative record of Holocene hydrological regime on the Heixiazi Island (NE China): indications for the evolution of East Asian summer monsoon. Clim. Dyn. 52 (11), 6773–6786.
Zhang, Z., Yao, Q., Liu, K.B., Xu, Q., Wang, G., 2020. Hydrological regime responses to Holocene East Asian summer monsoon circulation in marshes of the Sanjiang Plain, NE China. Land Degrad. Dev. 31 (2), 240–250.